Sensitivity of Heterointerfaces on Emission Wavelength of Quantum Cascade Lasers

C.A. Wang[1], B. Schwarz[2,3], D.F. Siriani[1], M. K.Connors[1], L.J. Missaggia[1], D.R. Calawa[1], D. McNulty[1], A. Akey[2], M.C Zheng[1], J.P. Donnelly[1], T. S. Mansuripur[2], and F. Capasso[2]

[1]MIT Lincoln Laboratory, Lexington, MA 02420-9108
[2]School of Engineering and Applied Sciences, Harvard University, Cambridge, MA 02138
[3]Institute for Solid State Electronics, TU-Wien, Vienna 1040, Austria

Abstract

The measured emission wavelengths of AlInAs/GaInAs/InP quantum cascade lasers (QCLs) grown by metal organic vapor phase epitaxy (MOVPE) have been reported to be ~ 0.5 to 1 μm longer than the designed QCL wavelength. This work clarifies the origin of the red-shifted wavelength. It was found that AlInAs/GaInAs heterointerfaces are compositionally graded over ~ 2.5 to 4.5 nm, and indium accumulates at the AlInAs-to-GaInAs interface. Thus, the as-grown QCLs are far from the ideal abrupt interfaces used in QCL modeling. When graded layers are incorporated in QCL band structure and wavefunction calculations, the emission wavelengths are red shifted. Furthermore, we demonstrate that QCLs with graded interfaces can be designed without compromising performance and show greatly improved correlation between designed and measured emission wavelength. QCLs were designed for emission at 7.5 and 8.5 μm. These QCLs exhibit room temperature peak power exceeding 900 mW and pulsed efficiencies of ~8.5 to 10%.

Keywords: A1. Interfaces, A1. Segregation, A3. Metalorganic vapor phase epitaxy, A3. Quantum wells, B2. Semiconducting III-V materials, B3. Infrared devices, B3. Quantum cascade lasers.

1. Introduction

Quantum cascade lasers (QCLs) [1] based on the AlInAs/GaInAs/InP materials system are optical sources that can be designed to operate at emission wavelengths over a wide wavelength range from the mid- to long-wave infrared (~3-25 μm). This versatility in wavelength design, coupled with watt-level continuous-wave output power [2-4], makes these compact lasers extremely attractive for a variety of applications including infrared (IR) countermeasures, free-space communications, and chemical and biological sensing. The QCL wavelength is determined by the energy separation of sub-band states in the conduction band of a coupled quantum-well structure, where the energy separation for a given material system and strain state is dependent on the thickness of the quantum wells and barriers. Thus, it is important to maintain precise control over alloy composition, layer thickness, and heterointerface quality of the many hundreds of ultra-thin epilayers (typically 0.6 to 5 nm thick) in the realization of high-performance QCLs with predictable emission wavelength.

Previously, it was reported that measured emission wavelengths of mid-wave and long-

wavelength infrared QCLs grown by metal organic vapor phase epitaxy (MOVPE) are ~0.5 to 1 μm longer than the calculated QCL wavelength [5-8]. It was proposed that the QCL red-shifted wavelength is due to indium surface segregation and graded interfaces [6]. That conclusion was based on the observation of increasing compressive strain with decreasing layer thickness, as measured by high-resolution x-ray diffraction (HRXRD), in AlInAs/GaInAs/InP superlattices. While indium segregation is qualitatively consistent with longer QCL emission wavelengths and HRXRD is useful in establishing MOVPE growth parameters to control the average strain in QCLs, further optimization of QCL performance is limited since quantitative measurements of individual layer compositions are not known. Thus, QCL modeling of bandstructure and energy levels can only assume nominal AlInAs barrier and GaInAs well alloy compositions and abrupt interfaces. In a recent report, the Al composition and layer thickness in QCL structures were calculated from intensity profiles of high-angle annular dark-field scan images that were obtained in scanning transmission electron microscopy and energy-dispersive x-ray spectroscopy [7]. It was found that many of the barrier layers are AlGaInAs quaternaries instead of AlInAs, and the Al content decreased with decreasing layer thickness. To correct the composition, a secondary flow of the Al precursor was added during MOVPE growth to increase Al content in QCLs. The resulting emission wavelength decreased.

The objective of this work is to investigate underlying factors that lead to non-idealities in the MOVPE growth of QCLs and clarify origins of the red-shifted wavelength offset in previously reported QCLs [5-8]. Results from a combination of in-situ and ex-situ characterization of a specially designed set of AlInAs/GaInAs multiple-quantum-well (MQW) structures, along with QCL modeling are presented. It was found that decreasing the AlInAs thickness (with constant GaInAs thickness) resulted in increasingly compressive structures, as measured by ex-situ HRXRD, while changes in GaInAs thickness (with constant AlInAs thickness) had no significant effect on overall strain. In-situ measurements of wafer curvature show that compressive strain accumulates at the AlInAs-to-GaInAs interface, but not at the GaInAs-to-AlInAs interface. These observations are further clarified by atomic concentration profiles of AlInAs/GaInAs heterointerfaces as measured by atom-probe tomography (APT). The data show that heterointerfaces are compositionally graded, with excess indium at the AlInAs-to-GaInAs interface. The GaInAs-to-AlInAs and AlInAs-to-GaInAs interfaces are asymmetric with a longer grading width at the GaInAs-to-AlInAs interface. The concentration profiles are consistent with indium surface segregation and lower indium solubility in AlInAs compared to GaInAs. Since the grading width is larger than individual layer thicknesses in the QCL, the nominal ternary composition is not obtained. The AlInAs barrier layers in the QCL active region, which are typically 0.1 nm or less, are particularly impacted, and bandstructure modeling results confirm that the laser transition energy is reduced and responsible for the red-shifted wavelength observed in our QCLs grown by MOVPE. Not all QCLs grown by MOVPE exhibit the same extent of difference from the intended design wavelength [9-11], and we also discuss growth parameters and processes that can be modified to significantly affect interface grading and indium surface segregation.

2. Experimental Methods

AlInAs/GaInAs multiple quantum well (MQW) structures and QCLs were grown on

(100) n-InP substrates by MOVPE in a Veeco D125 multi-wafer (3x2) reactor with 28 slpm H_2 as the carrier gas and reactor pressure of 60 T. Trimethylaluminum (TMAl), trimethylgallium (TMGa), and trimethylindium (TMIn) were used for group III precursors, and phosphine and arsine as group V precursors. Si_2H_6 (diluted 200 ppm in H_2) was used as the n-type dopant. The growth temperature was 625 °C as measured by emissivity corrected optical pyrometrey. AlInAs and GaInAs were grown with a single TMIn source at a growth rate of ~0.3 nm/s. No growth interrupts were used between AlInAs and GaInAs interfaces. InP layers were grown at a higher rate of 0.6-0.7 nm/s. The V/III ratios were ~90 for AlInAs and GaInAs, and ~130 for InP. All epilayer structures were grown nominally lattice matched (strain less than 0.2%) to the (100) n-InP substrates, doped 2-5 x $10^{18}cm^{-3}$. A limited number of growth runs were performed with an EpiCurveTT in-situ optical system to simultaneously monitor epilayer growth at 450 nm reflectance and wafer curvature. The structures were characterized ex-situ by high-resolution x-ray diffraction (HRXRD). Average layer strain and MQW period thickness was determined using Philips X'pert software (PANalytical Inc.). APT was used to measure chemical composition at heterointerfaces.

QCLs were fabricated by conventional photolithography and wet etching techniques. The ridge lasers were either 20 or 25 μm in width. Following the wet etching, the side-walls were electrically insulated with a 0.3 µm-thick SiN_x dielectric layer. Ti-Au metallization was used for top and back contact. Lasers were cleaved into 3-mm-long bars and the facets were uncoated. QCLs were probe tested as fabricated in chip form on a temperature-controlled stage at 15 °C. Laser testing was performed under low-duty factor pulsed conditions, 200 ns at a repetition frequency of 1 kHz. The laser power was coupled into an integrating sphere with HgCdTe detector (Vigo PCI-3TE-12). Power calibration of the photodetector signal was made by measuring the laser power using a thermal detector. The lasing wavelength was measured using a Fourier-transform infrared spectrometer.

3. Results and Discussion

3.1 Heterointerfaces in AlInAs/GaInAs MQWs

A series of AlInAs/GaInAs MQWs was grown in which either the AlInAs barrier or the GaInAs well layer thickness (d_B or d_W, respectively) was separately reduced so that interface effects at AlInAs-to-GaInAs or GaInAs-to-AlInAs heterointerfaces could be independently revealed. By maintaining d_B constant and reducing d_W, it is possible to study the GaInAs-to-AlInAs transition. Similarly, with d_W held constant while reducing d_B, the AlInAs-to-GaInAs transition can be studied. Details of the MQW samples with various layer thickness changes are listed in Table 1. Layer thicknesses were varied from 10 to 1.25 nm. The number of MQW periods was changed in order to keep the total layer thickness at ~0.4 μm.

The HRXRD scans of the MQWs are shown in Figure 1 and are aligned with the InP substrate peak at 0 rel arc sec and offset for clarity. The scan from the thickest barrier and well layers ($d_B = d_W = 10$ nm) is the bottom (sample a), and either d_W or d_B is decreasing towards the top. The spacing of satellite peaks increases as the period decreases as expected, and all scans exhibit sharp satellite peaks and highly resolved thickness interference fringes. The full-width at

half-maximum of the n=0 peak is nominally similar for all MQWs. It ranges between 41.8 arc sec for the 20-nm-period MQW (sample a) and 44.7 arc sec for the 3.75-nm-period MQW (sample f). These results indicate that the interfaces are well-defined and very flat with excellent repeatability in thickness and composition throughout the structure, even for sample f with d_B as thin as 1.25 nm.

Also to be noted in Figure 1 is the position of the zeroth order satellite (n=0 peak near the substrate peak), which determines the average perpendicular lattice parameter. The n=0 peak position is listed in Table 1. For samples a-c with d_B = 10 nm and varying d_W from 10 to 2.5 nm (GaInAs-to-AlInAs interface), the n=0 peak position is nominally similar. However, for samples c-f with constant d_W = 2.5 nm and varying d_B from 10 to 1.25 nm (AlInAs-to-GaInAs interface), the n=0 peak position moves toward lower negative diffraction angles and indicates a systematic trend toward more compressively strained structures. The change in strain with either d_B or d_W is plotted in Figure 2, where the data have been referenced to sample a with 10-nm-thick AlInAs and GaInAs layers. Varying d_W with constant d_B has a negligible effect on the change in strain, while varying d_B with constant d_W results in a dramatic increase of nearly 0.15% compressive strain. This compressive strain is likely due to interfacial strain that accumulates at the AlInAs-to-GaInAs heterointerface.

It has been reported that strain accumulation in InGaAs/GaAsP strain-balanced MQWs can be effectively monitored during growth by in-situ wafer curvature measurement [12, 13]. Therefore, to further investigate the origin of compressive strain accumulation in our nominally lattice-matched AlInAs/GaInAs MQWs, we used in-situ optical monitoring during the growth of MQW test structures to probe both the GaInAs-to-AlInAs and AlInAs-to-GaInAs heterointerfaces. In one experiment, d_B was constant at 10 nm while d_W was reduced from 10 to 0.65 nm (GaInAs-to-AlInAs interface). In the other experiment, d_W was constant at 10 nm while d_B was reduced from 10 to 1.25 nm (AlInAs-to-GaInAs interface). The number of periods was increased as the period thickness decreased. The reflectance, monitored at 450 nm, and wafer curvature from the two growth runs are shown in Figure 3. Reflectance oscillations correspond to the each barrier and well layer and each layer is easily resolved. For the growth run shown in Figure 3a with decreasing d_W with constant d_B, wafer curvature is relatively constant. However, for the structure with decreasing d_B with constant d_W (Figure 3b), the wafer curvature becomes increasingly negative when d_B is reduced below 5 nm. The increase in negative curvature is due to the accumulation of compressive strain at the AlInAs-to-GaInAs interface. These results are consistent with the ex-situ HRXRD data obtained for the series of MQWs listed in Table 1 and previously discussed, providing further support that compressive strain accumulates at the AlInAs-to-GaInAs heterointerface.

APT is a nano-characterization technique that has the ability to map chemical compositions on an atomic spatial scale, and has been demonstrated to be particularly useful in characterizing interfaces in multilayer films [14]. APT was used to analyze AlInAs/GaInAs heterointerfaces, and cation profiles are presented in Figure 4. The As profile has not been plotted for clarity. The cation fractions of Ga and In in GaInAs are around the nominally lattice matched values ($Ga_{0.53}In_{0.47}As$), while the composition of AlInAs corresponds to about 0.5% tensile strain ($Al_{0.52}In_{0.48}As$ is lattice matched). The data show that the heterointerfaces are compositionally graded, and the grading width is asymmetric at AlInAs-to-GaInAs and GaInAs-

Commented [ID1]: Does the As profile show anything interesting? Does it provide any support to the story?

Commented [CAW2]: Nothting to support segregation.

4

to-AlInAs interfaces. The width of the AlInAs-to-GaInAs transition is 2.5 nm compared to a transition width of 4.5 nm at the GaInAs-to-AlInAs interface. In addition, there is an abrupt increase in excess indium (0.57) at the AlInAs-to-GaInAs interface, which then decreases over ~0.8 nm to the steady value in the GaInAs layer. The In-rich region will lead to interfacial compressive strain at the AlInAs-to-GaInAs interface. The width of this interfacial layer is relatively constant. Thus as d_B is reduced, the extent of the In-rich region becomes an increasingly greater fraction of the period thickness, and contributes more in the average strain in the structure. As shown in the ex-situ and in-situ measurements of strain in the MQWs discussed in Figures 1-3, compressive strain increases with decreasing d_B.

We attribute both the excess indium and asymmetrically graded interfaces to indium surface segregation whereby an In-rich region tends to form at the growing surface, and the tendency for indium surface segregation is higher in AlInAs than GaInAs [15-17]. Indium surface segregation has been observed in both molecular beam epitaxy (MBE) [15, 17-19] and MOVPE [20] and leads to interface broadening. Segregation lengths of 2.9 nm are reported for MBE [19] and 3-4 nm for MOVPE [20]. Based on the results of this work and surface segregation studies, the AlInAs surface is enriched in indium during growth. When GaInAs is grown on top of AlInAs, the indium surface atoms incorporate into the GaInAs since it has a higher solubility for indium than AlInAs. Subsequently, when AlInAs is grown on GaInAs, indium incorporation is slower and this leads to a wider grading length for GaInAs-to-AlInAs compared to AlInAs-to-GaInAs.

It is important to point out that even in the absence of surface segregation, heterointerfaces can be compositionally graded in MOVPE-grown heterostructures due to gas diffusion and hydrodynamic dispersion in the MOVPE reactor [21, 22]. Dispersion is a fundamental process operating in MOVPE and smears out the compositional gas front so that the concentration at the wafer surface exhibits a transient before reaching its steady state value rather than exhibiting an abrupt step change. The time required to reach steady state concentration depends mainly on the gas residence time. Growth parameters that can minimize interfacial grading include reducing the gas residence time, reducing the epilayer growth rate, and adding a growth interruption at each heterointerface.

It is also recognized that not all MOVPE-grown QCLs have been reported to exhibit red-shifted emission wavelengths. In those reports [9-11], the growth conditions were more conducive to reducing indium surface segregation and hydrodynamic dispersion effects. Such parameters included reduced gas residence time via reactor geometry [9, 10], higher V/III ratios than used in this study [9-11,19], high growth temperatures [10, 20, 23], very low growth rates of 0.1 nm/s [9] or growth interruptions [9, 11] .

On the other hand, growth conditions could be more conducive indium segregation compared to the conditions used in this study. It is was reported in [6] that the QCL emission wavelength was red-shifted ~1 μm. Those QCLs were grown by MOVPE with tertiarybutyl arsine as the group V, precursor and the V/III ratio was only 5. In that work, MQW test structures showed an increase in compressive strain with not only decreasing d_B, but also decreasing d_W. Thus, it is highly probable that indium surface segregation was operative in both the AlInAs and GaInAs under the growth conditions used in that work.

3.2 QCL Devices

In order to further study the impact of compositional interface grading as well as obtain better correlation between experimentally measured and calculated QCL wavelengths, QCLs were modeled to account for graded interfaces, grown, and evaluated. As a first approximation and to first establish the method, a relatively simple model was adopted to represent intermixing between AlInAs and GaInAs. The resulting graded interface produces a quaternary alloy AlGaInAs, where the function $1/(1+\exp(x/L))$ defines the mixture between lattice-matched GaInAs and AlInAs. A barrier has then the concentration shape $1/(1+\exp((x-d_B)/L)) - 1/(1+\exp(x/L))$, where L is the grading width. While this is an oversimplification of the compositional profiles shown in Figure 4, there are many additional unknown parameters that could further influence energy levels. L was empirically determined from in-house historically measured QCL electroluminescence wavelengths to be 0.22 nm.

A QCL based on single-phonon continuum depopulation [24] was adopted as the baseline structure for study, as this scheme yields high device performance and is robust against layer-thickness fluctuations. The AlInAs/GaInAs layer sequence of one period starting from the injection barrier is as follows:
3.8/1.5/**0.9**/5.3/**0.8**/5.2/**0.9**/4.8/**1.6**/3.7/**2.2**/3.0/**1.8**/2.8/**1.9**/2.7/**2.0**/2.6/**2.5**/2.7/**3.1**/2.5. The AlInAs barrier layers are in bold print, and the underlined layers are Si-doped injector layers. A comparison of the bandstructure and moduli squared of the wavefunctions in the active region in which the barrier and well layers are compositionally abrupt or graded are shown in Figures 5a and 5b, respectively. The grading has a dramatic change on the alloy composition and energy levels in the active region, where the three barrier layers have the quaternary AlGaInAs composition. The calculated transition energy for the QCL with abrupt interfaces corresponds to a wavelength of 8.2 μm. With the graded interfaces, energy barrier heights are lower and consequently the lasing transition energy is reduced by 15 meV, or equivalently a lasing wavelength of 9.1μm. These results show that the graded interfaces can be responsible for red-shifted QCL emission wavelengths.

To further support this hypothesis, a series of QCLs were designed with the same graded interfaces. Bandstructures of QCLs designed for emission at 7.5 and 8.5 μm are shown in Figure 6. QCLs were grown with 35 periods and injector sheet doping of ~1.1×10^{11} cm^{-2}. The lower and upper InP cladding layer thickness was 3.5 μm, and was Si doped 5×10^{16} cm^{-3}. GaInAs waveguide layers were Si doped 2×10^{16} cm^{-3} and were 0.5 μm thick. A heavily Si-doped ($>5 \times 10^{18}$ cm^{-3}) plasmon-confinement layer was 0.5 μm thick, followed by a 0.2 μm-thick GaInAs contact layer ($>2 \times 10^{19}$ cm^{-3}).

Pulsed light-current (L-I) and voltage-current (V-I) characteristics of uncoated QCL devices are shown in Figure 7, and the insets shown the lasing spectrum. The 7.5 μm laser has a threshold current density J_{th} of 0.85 kA/cm^2, slope efficiency/facet of 0.82 W/A, and maximum total power conversion efficiency η_{max} of 8.2%. The 8.5 μm laser has a slightly higher threshold current density J_{th} of 1.1 kA/cm^2, slope efficiency/facet of 0.85 W/A, and maximum total power

Commented [ID3]: Is this right?

Commented [CAW4]: This is sheet density, so I added 'sheet.'

conversion efficiency η_{max} of 10%. Both devices emit over 900 mW/facet of peak output power. The lasing wavelength of these devices is 7.46 and 8.5 µm and very well correlated with the design wavelength. In addition, a QCL was designed for 8.0 µm emission. The measured emission wavelength was 8.0 µm, and similar high performance with η_{max} of 9.4%. The performance of these devices with graded heterointerfaces is comparable or slightly better than the pulsed performance reported in [24], and thus, QCLs with graded interfaces can operate with no compromise in performance.

4. Summary

This work investigates the origin of the measured red-shifted emission wavelengths of AlInAs/GaInAs/InP QCLs grown by MOVPE, as compared to calculated QCL wavelengths. AlInAs/GaInAs multiple quantum well (MQW) test structures were grown by MOVPE with successively decreasing barrier and well layers to reveal heterointerface effects. It was found from both in-situ optical monitoring and ex-situ HRXRD that decreasing the AlInAs thickness resulted in increasingly compressive structures, while changes in GaInAs thickness barely affected overall strain. APT revealed compositionally graded interfaces and indium accumulation at the AlInAs-to-GaInAs interface. The GaInAs-to-AlInAs and AlInAs-to-GaInAs interfaces are asymmetric due to this indium surface segregation, with more interfacial grading at the GaInAs-to-AlInAs interface. QCL modeling of graded interfaces clearly indicates that the barrier layers in the QCL active region are AlGaInAs instead of AlInAs, and the calculated emission wavelength is red-shifted compared to structures modeled with abrupt ternary heterointerfaces. Even if indium surface segregation can be eliminated, attainment of compositionally abrupt heterointerfaces grown using MOVPE will be fundamentally limited by hydrodynamic dispersion. In addition, we demonstrate greatly improved agreement between designed and measured emission wavelength in QCLs operating at 7.5 and 8.5 μm, with high-performance QCLs exhibiting room temperature peak power exceeding 900 mW and pulsed efficiencies of ~8.5 to 10%.

References

[1]   J. Faist, F. Capasso, D. L. Sivco, C. Sirtori, A. L. Hutchinson, and A. Y. Cho, "Quantum Cascade Laser," *Science*, vol. 264, pp. 553-556, 1994.

[2]   A. Lyakh, R. Maulini, A. G. Tsekoun, and C. K. N. Patel, "Progress in high-performance quantum cascade lasers," *Optical Engineering*, vol. 49, pp. 111105-8, 2010.

[3]   M. Razeghi, Y. Bai, S. Slivken, and S. R. Darvish, "High-performance InP-based midinfrared quantum cascade lasers at Northwestern University," *Optical Engineering*, vol. 49, pp. 111103-4, 2010.

[4]   A. Lyakh, R. Maulini, A. Tsekoun, R. Go, and C. K. N. Patel, "Multiwatt long wavelength quantum cascade lasers based on high strain composition with 70% injection efficiency," *Opt. Express*, vol. 20, pp. 24272-24279, 2012.

[5]   C. A. Wang, R. K. Huang, A. Goyal, J. P. Donnelly, D. R. Calawa, S. G. Cann, F. O'Donnell, J. J. Plant, L. J. Missaggia, G. W. Turner, and A. Sanchez-Rubio, "OMVPE growth of highly strain-balanced GaInAs/AlInAs/InP for quantum cascade lasers," *Journal of Crystal Growth*, vol. 310, pp. 5191-5197, 2008.

[6]   C. A. Wang, A. K. Goyal, S. Menzel, D. R. Calawa, M. Spencer, M. K. Connors, D. McNulty, A. Sanchez, G. W. Turner, and F. Capasso, "High power (>5 W) λ~9.6 μm tapered quantum cascade lasers grown by OMVPE," *Journal of Crystal Growth*, vol. 370, pp. 212-216, 2013.

[7]   P. Konstantinos, B. Grégoire, P. Gilles, L. Ludovic, M. Olivia, P. Giulia, V. Angela, C. Ariane, A. Maria, S. Carlo, and S. Isabelle, "Sub-nanometrically resolved chemical mappings of quantum-cascade laser active regions," *Semiconductor Science and Technology*, vol. 31, pp. 055017, 2016.

[8]   L. Missaggia, C. Wang, M. Connors, B. Saar, A. Sanchez-Rubio, K. Creedon, G. Turner, and W. Herzog, "Thermal management of quantum cascade lasers in an individually addressable monolithic array architecture," Proc. SPIE vol. 9730, pp.973008, 2016.

[9]   D. Bour, M. Troccoli, F. Capasso, S. Corzine, A. Tandon, D. Mars, and G. Hofler, "Metalorganic vapor-phase epitaxy of room-temperature, low-threshold InGaAs/AlInAs quantum cascade lasers," *Journal of Crystal Growth*, vol. 272, pp. 526-530, 2004.

[10]   Y. Huang, J.-H. Ryou, R. D. Dupuis, C. Pflügl, F. Capasso, K. Sun, A. M. Fischer, and F. A. Ponce, "Optimization of growth conditions for InGaAs/InAlAs/InP quantum cascade lasers by metalorganic chemical vapor deposition," *Journal of Crystal Growth*, vol. 316, pp. 75-80, 2011.

[11]   J. C. Shin, L. J. Mawst, and D. Botez, "Crystal growth via metal–organic vapor phase epitaxy of quantum-cascade-laser structures composed of multiple alloy compositions," *Journal of Crystal Growth*, vol. 357, pp. 15-19, 2012.

[12]   M. Sugiyama, K. Sugita, Y. Wang, and Y. Nakano, "In situ curvature monitoring for metal-organic vapor phase epitaxy of strain-balanced stacks of InGaAs/GaAsP multiple quantum wells," *Journal of Crystal Growth*, vol. 315, pp. 1-4, 2011.

[13]   S. Ma, Y. Wang, H. Sodabanlu, K. Watanabe, M. Sugiyama, and Y. Nakano, "Effect of hetero-interfaces on in situ wafer curvature behavior in InGaAs/GaAsP strain-balanced MQWs," *Journal of Crystal Growth*, vol. 352, pp. 245-248, 2012.

[14]   T. F. Kelly and M. K. Miller, "Atom probe tomography," *Review of Scientific Instruments*, vol. 78, pp. 031101, 2007.

[15] J. M. Moison, C. Guille, F. Houzay, F. Barthe, and M. Van Rompay, "Surface segregation of third-column atoms in group III-V arsenide compounds: Ternary alloys and heterostructures," *Physical Review B*, vol. 40, pp. 6149 LP - 6162, 1989.

[16] J.-M. Gerard, "In situ probing at the growth temperature of the surface composition of (InGa)As and (InAl)As," *Applied Physics Letters*, vol. 61, pp. 2096-2098, 1992.

[17] G. Grenet, E. Bergignat, M. Gendry, M. Lapeyrade, and G. Hollinger, "In situ XPS investigation of indium surface segregation for $Ga_{1-x}In_xAs$ and $Al_{1-x}In_xAs$ alloys grown by MBE on InP(001)," *Surface Science*, vol. 352-354, pp. 734-739, 1996.

[18] J. M. Moison, F. Houzay, F. Barthe, J. M. Gérard, B. Jusserand, J. Massies, and F. S. Turco-Sandroff, "Surface segregation in III-V alloys," *Journal of Crystal Growth*, vol. 111, pp. 141-150, 1991.

[19] K. Muraki, S. Fukatsu, Y. Shiraki, and R. Ito, "Surface segregation of In atoms during molecular beam epitaxy and its influence on the energy levels in InGaAs/GaAs quantum wells," *Applied Physics Letters*, vol. 61, pp. 557-559, 1992.

[20] A. A. Marmalyuk, O. I. Govorkov, A. V. Petrovsky, D. B. Nikitin, A. A. Padalitsa, P. V. Bulaev, I. V. Budkin, and I. D. Zalevsky, "Investigation of indium segregation in InGaAs/(Al)GaAs quantum wells grown by MOCVD," *Journal of Crystal Growth*, vol. 237-239, pp. 264-268, 2002.

[21] C. A. Wang, S. Patnaik, J. W. Caunt, and R. A. Brown, "Growth characteristics of a vertical rotating-disk OMVPE reactor," *Journal of Crystal Growth*, vol. 93, pp. 228-234, 1988.

[22] S. Patnaik, R. A. Brown, and C. A. Wang, "Hydrodynamic dispersion in rotating-disk omvpe reactors: Numerical simulation and experimental measurements," *Journal of Crystal Growth*, vol. 96, pp. 153-174, 1989.

[23] J. Massies, F. Turco, A. Saletes, and J. P. Contour, "Experimental evidence of difference in surface and bulk compositions of AlxGa1-xAs, AlxIn1-x As and GaxIn1-x As epitaxial layers grown by molecular beam epitaxy," *Journal of Crystal Growth*, vol. 80, pp. 307-314, 1987.

[24] K. Fujita, S. Furuta, A. Sugiyama, T. Ochiai, T. Edamura, N. Akikusa, M. Yamanishi, and H. Kan, "High-Performance λ ~ 8.6 μm Quantum Cascade Lasers With Single Phonon-Continuum Depopulation Structures," *Quantum Electronics, IEEE Journal of*, vol. 46, pp. 683-688, 2010.

Table 1. Details of AlInAs/GaInAs MQW structures. Samples were grown without growth interruption.

Sample	Barrier thickness (nm)	Well thickness (nm)	SL period	Number of periods	n=0 peak position (rel arc s)
a	10	10	20	20	199
b	10	5	15	26	194
c	10	2.5	12.5	32	176
d	5	2.5	7.5	52	95
e	2.5	2.5	5	80	-36
f	1.25	2.5	3.75	100	-140
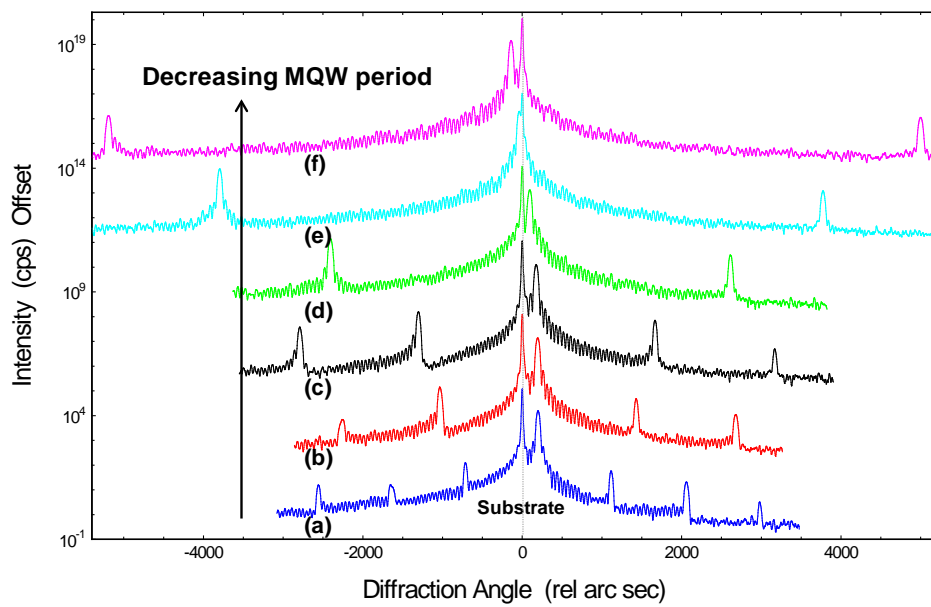
Figure 1. High-resolution x-ray diffraction scans of AlInAs/GaInAs MQWs listed in Table 1: (a) 10/10 nm (x20); (b) 10/5 nm (x26); (c) 10/2.5 nm (x32); (d) 5/2.5 nm (x52); (e) 2.5/2.5 nm (x80); (f) 1.25/2.5 nm (x100).
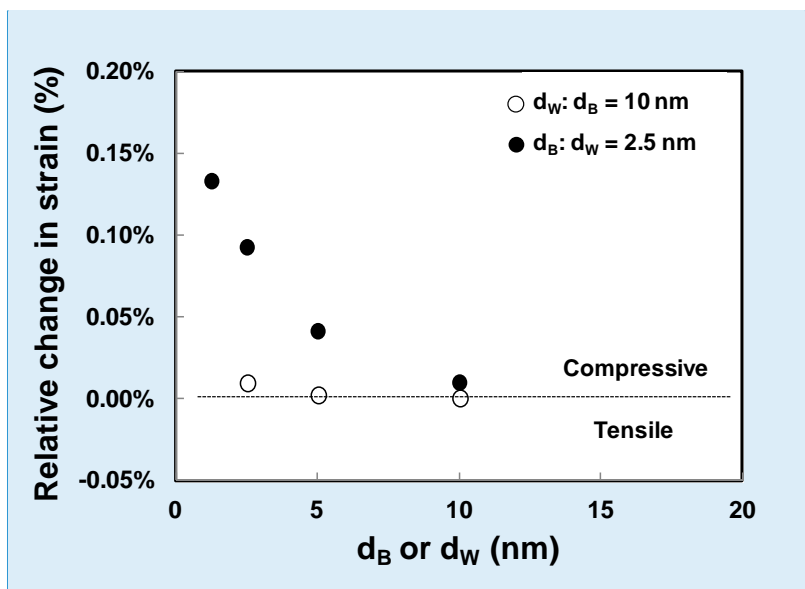
11

Figure 2. Relative change in strain of AlInAs/GaInAs MQWs grown with constant $d_B = 10$ nm (open circles) and varying d_W or constant $d_W = 2.5$ nm (filled circles) and varying d_B.
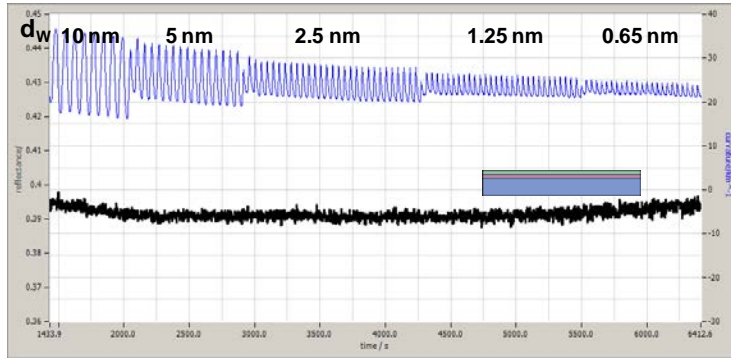
(a)
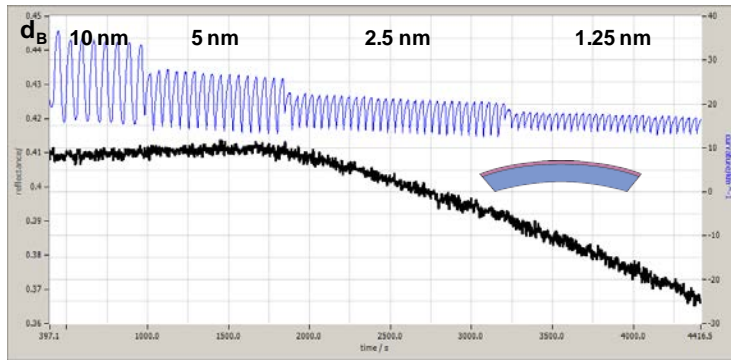
(b)

Figure 3. In-situ optical monitoring of AlInAs/GaInAs MQWs: reflectance at 450 nm (upper curve) and wafer curvature (lower curve). (a) Varying d_W with constant $d_B = 10$ nm and (b) varying d_B with constant $d_W = 10$ nm.
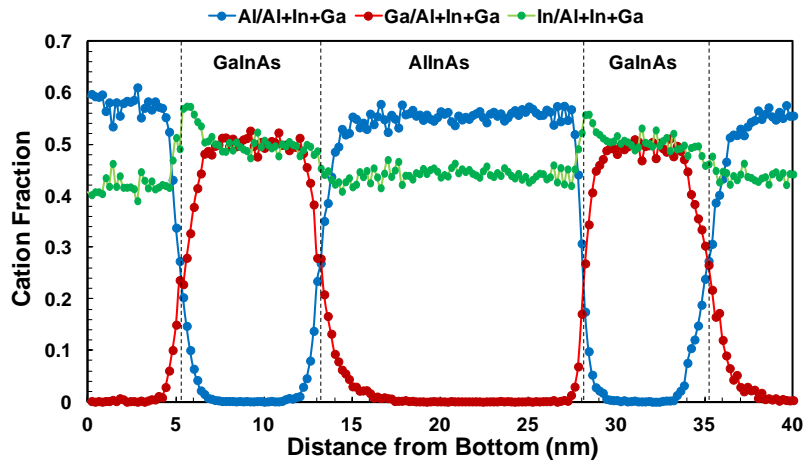
Figure 4. Cation concentration profiles of Al, Ga, and In in AlInAs/GaInAs MQW. The growth direction is from left to right.

(a) (b)
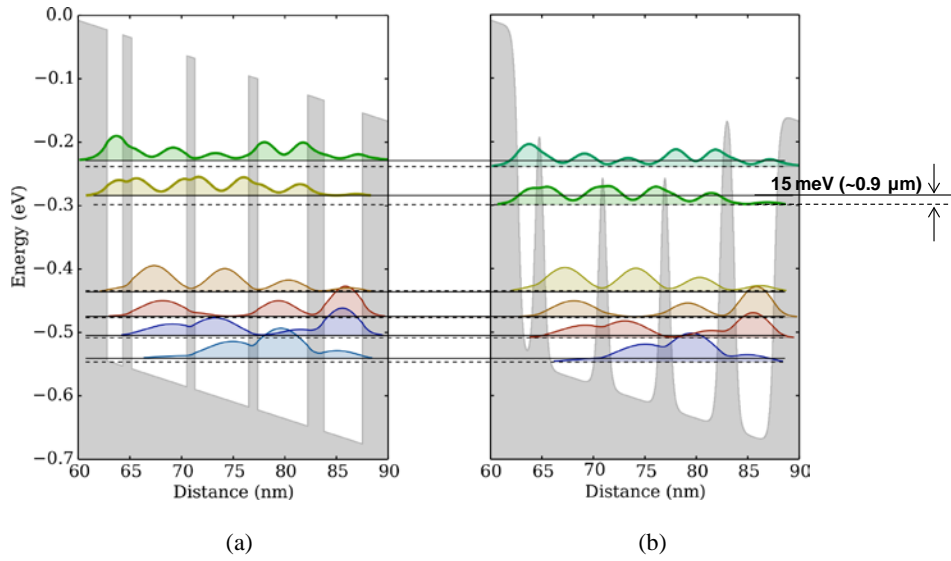
Figure 5. Calculated conduction band diagram and moduli squared of the wave functions for the active region of the QCL with compositionally (a) abrupt interfaces (8.2 μm lasing transition) and (b) graded interfaces (9.1 μm lasing transition). The barrier heights of the three thinner barrier layers are considerably lower and consequently the lasing transition energy is reduced by 15 meV.
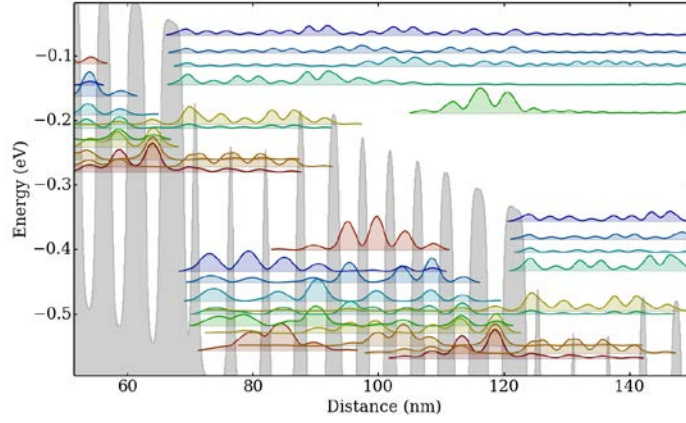
(a)
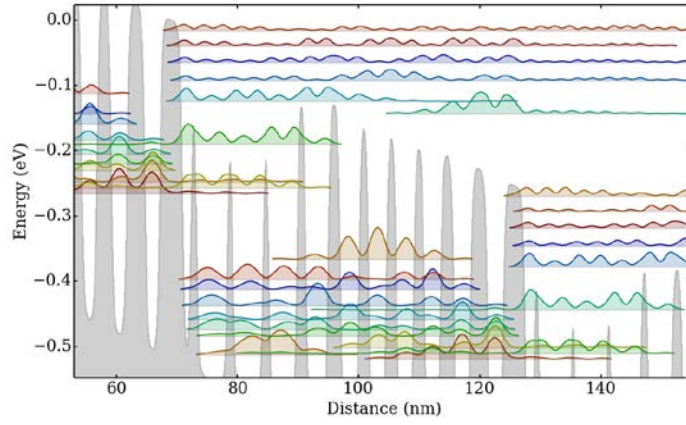
(b)

Figure 6. Calculated conduction band diagram and moduli squared of the wave functions for QCLs designed for (a) 7.5 μm and (b) 8.5 μm emission. The AlInAs/GaInAs layer sequence of one period starting from the injection barrier is as follows:
(a)   **4.1**/1.1/**1.1**/4.65/**0.95**/4.55/**1.05**/4.2/**1.7**/3.3/**2.3**/2.5/**1.9**/2.4/**2.0**/2.3/**2.2**/2.1/**2.7**/2.15/**3.3**/2.0;
(b) **3.9**/1.3/**0.95**/5.1/**0.85**/5.0/**0.95**/4.6/**1.6**/3.5/**2.2**/2.9/**1.8**/2.7/**1.9**/2.6/**2.0**/2.4/**2.5**/2.45/**3.1**/2.3. The AlInAs barrier layers are in bold print, and the underlined layers are Si-doped injector layers.
The AlInAs barrier layers are in bold print, and the underlined layers are Si-doped injector layers.

16
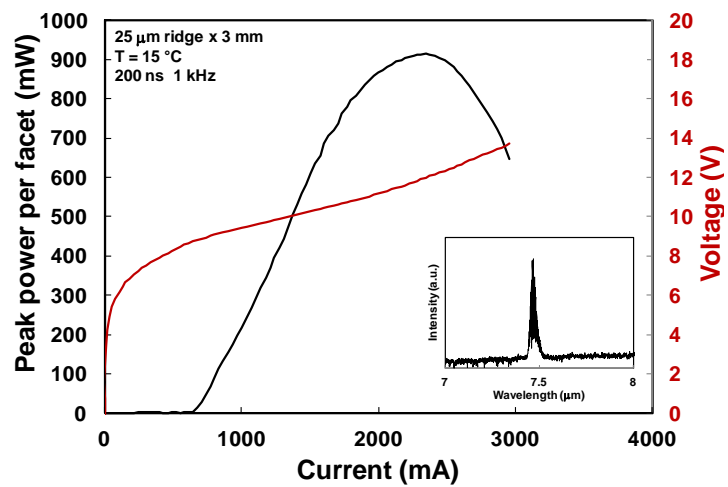
(a)
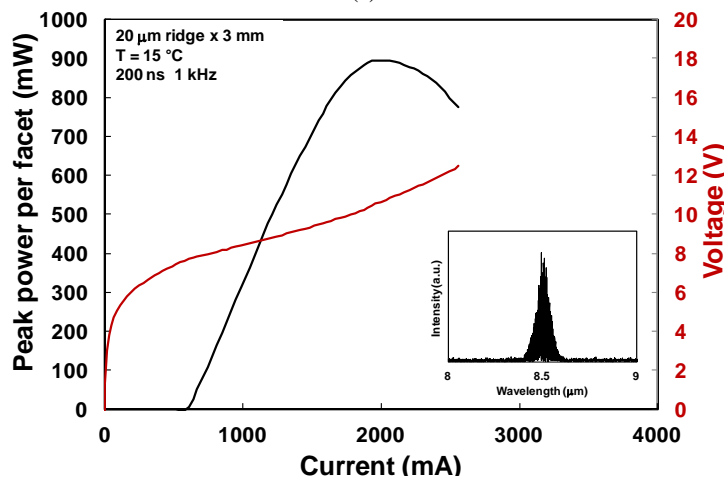
(b)

Figure 7. Room-temperature pulsed power-current-voltage characteristics of uncoated QCL ridge (a) 7.5 µm design and (b) 8.5 µm design. Measurements were made on unmounted bars under pulsed conditions.